Influence of Atmospheric Corrosivity on the Seismic Fragility of Low-code Steel Frame Structures

Devang Lad[1], Fabio Freddi[1] and Jayadipta Ghosh[2]

[1] University College London, London, U.K.
[2] Indian Institute of Technology Bombay, Mumbai, India
devang.lad.21@ucl.ac.uk

Abstract. Low-code steel moment-resisting frames (pre-Northridge) are characterised by high seismic vulnerability due to their reduced ductility capacity. Moreover, these structures are exposed to atmospheric corrosion deterioration due to environmental corrosive agents. Corrosion deterioration leads to section mass loss, stiffness degradation, and loss of energy dissipation capacity, among others. Thus, based on the corrosive category, old steel structures could experience considerable variations in their seismic performance. The present study examines the effect of different corrosivity categories on the seismic vulnerability of steel frames. A non-seismically designed three-storey moment-resisting frame is selected for case-study purposes and exposed to increasing corrosivity categories (C3, C4, C5, and CX) as per ISO 9223: 2012. As per ISO 9224:2012, atmospheric corrosion is assessed considering a 50-year ageing time and uniform corrosion. The seismic performance of the pristine and ageing steel frames is evaluated through Incremental Dynamic Analyses (IDAs) considering a suite of 43 ground motion records to account for the record-to-record variability. The seismic performance under different exposure categories is evaluated by monitoring local and global engineering demand parameters (*EDPs*), allowing the development of seismic fragility functions at components- and system-levels.

Keywords: Existing steel frame, Atmospheric corrosion, Corrosivity Categories, Local engineering demand parameters, Fragility curves.

1 Introduction

Steel moment resisting frames (MRFs) designed and erected prior to the implementation of seismic design codes exhibit high seismic vulnerability due to various deficiencies in design philosophy. The 1994 Northridge and 1995 Kobe earthquakes caused severe irreversible damage to steel structures and exposed several shortcomings [1]. These include weak panel zones, brittle welding zones, absence of capacity design, low ductility, and inadequate energy dissipation capacity [2].

In addition to the earthquake hazard, existing low-code steel structures may also be exposed to atmospheric corrosion deterioration, further exacerbating their seismic vulnerability. Experimental studies on corroded beam-column subassemblage have high-

lighted an adverse reduction of ductility and energy dissipation capacity [3]. The primary effects relate to the mass loss of steel sections due to the formation of rust. On the other hand, the secondary effects relate to the degradation in the mechanical properties of steel (*i.e.*, yield strength, modulus of elasticity) [4].

Past studies have mainly focused on assessing the seismic performance of bridges and infrastructures [5,6], while only a limited number of research works have focused on building structures. Among others, Shekhar *et al.* (2023) [7] examined the influence of chloride-induced corrosion on the change in failure mechanism for low-code reinforced concrete (RC) frames. Dizaj *et al.* (2018) [8] examined the seismic fragility of ductile and low-ductile RC frames subjected to non-uniform corrosion. A few other studies on RC frames exist. On the contrary, the literature focusing on steel structures is more restricted, and most studies investigated the response of isolated components (*e.g.*, corroded beam-column connections and cantilever column frames [9]). Some studies focusing on the global seismic response of corroded steel structures include Di Sarno *et al*. (2021) [10], who examined corrosion effects on the seismic performance of petrochemical building (high-rise) structures exposed to varying corrosive environments [11]. Results revealed that the storey acceleration for a very high corrosion level (C4 category) at 100 years is higher by 400% to 800% compared to a lower corrosion level (C3 and C4 category). Zhang *et al*. (2020) [12] explored the effect of varying corrosion levels on the seismic response of a three-storey single-bay steel frame both experimentally and numerically. The results showed that a corrosion mass loss (η) of 10.13% resulted in 21.8%, 12.2% and 23.9% reductions in maximum lateral load, global displacement ductility and interstorey drift ratio, respectively. The above literature and a few other numerical studies neglected taking into account for the beam-to-column joint modelling and corrosion. Furthermore, most studies focused on the global seismic response of corroded structures. To the authors' knowledge, no research has examined corrosion effects considering local engineering demand parameters (*EDPs*).

To address these knowledge gaps, the authors of this paper [4] previously investigated the corrosion impact on a three-storey low-code steel MRF with welded joints, considering a 50-year ageing time and the C4 exposure category. This case study building has been selected to be representative of a large amount of steel construction in seismic areas worldwide. Seismic fragility curves at component level were developed, revealing a 17% increase in column fragility corresponding to a 6.8% mass loss. The present paper expands the previous study by examining the fragility variations of the same case study frame, considering local *EDPs* and different corrosivity categories.

Various atmospheric conditions (C3, C4, C5, and CX) over a 50-year period are considered according to ISO 9223:2012 [11] corrosivity definitions. A time-dependent corrosion deterioration model based on ISO 9224:2012 [13] estimates corrosion damage. Uniform corrosion is assumed on columns and panel zones, accompanied by degradation in mechanical properties. A finite element (FE) model in OpenSees [14] is used to perform non-linear static and dynamic analyses, including Incremental Dynamic Analyses (IDAs) with a suite of 43 ground motion (GM) records to account for record-to-record variability. Finally, seismic fragility functions are developed at both system and component levels to evaluate and discuss the effects of the corrosivity category on the seismic performance of the case study structure.

2 Atmospheric corrosion and finite element (FE) modelling of the case-study structure

2.1 Case Study Structure

Boston's three-storey building (3B) from the SAC-FEMA project, designed as per the National Building Code (12th edition), has been adopted as a case-study structure [1]. The building is built on stiff soil with steel grade ASTM 572, and features a regular floor plan layout. The case-study structure is representative of typical low-rise, low-code buildings designed based on pre-Northridge design provisions. Thus, the building lacks capacity-based design considerations and is characterised by low-ductile joints. The plan and elevation views of the structure are shown in Fig. 1. The perimeter seismic-resistant steel MRF considered in this study is represented by the thick lines in Fig. 1(a), while its elevation view is shown in Fig. 1(b). The seismic masses for the 1st, 2nd, and 3rd storey are 956.6, 956.6, and 1035 tons, respectively. Only half of each storey mass is assigned in the FE model for a single perimeter frame (*i.e.*, two perimeter MRFs in the x-direction). The seismic risk category II (*e.g.*, small office building), according to ASCE 7-16 [15], is adopted for the case-study structure. Additional details regarding the case-study structure are provided by Gutiérrez-Urzúa *et al*. (2021) [2]. The case-study structure is assumed to be located in areas characterised by different corrosive categories. No corrosion protection coating is assumed. The assessment is done by comparing the pristine and 50-year-old frames exposed to different corrosive categories.

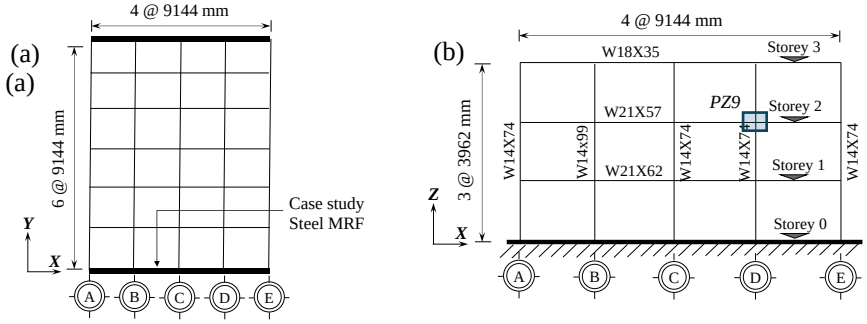

Fig. 1. Case study steel moment resisting frame (MRF): (a) Plan view; (b) Elevation view.

2.2 Atmospheric corrosion deterioration modelling

Atmospheric corrosion is an electrochemical reaction where steel is converted into rust, ultimately leading to thickness loss. This study assumes uniform corrosion in steel members for corrosion damage [10]. The corrosion rate (i_{corr}) in μm/year is used to quantify the damage (thickness loss) over a period of time. The corrosion rate (i_{corr}), or the first-year corrosion rate, reflects the complex relationships in the specific environmental situation of the year of exposure. Since the aim is to study the impact of different atmospheric environments; the case-study structure is assumed to be exposed

to four corrosivity categories: C3 (medium), C4 (high), C5 (very high), and CX (extreme). The range of corrosion rate as provided in ISO 9223:2012 [11] for carbon steel based on exposure test is presented in Table 1. This study adopts the average value from the range provided in Table 1 as the 'Avg.i_{corr}' value.

The thickness loss in the member section due to corrosion is estimated using the time-dependent corrosion loss model from ISO 9224:2012 [13], given by:

$$d(t \leq 20y) = i_{corr} t^B$$
$$d(t > 20y) = i_{corr}[20^B + B(20^{B-1})(t - 20)] \quad (1)$$

where, i_{corr} is the first-year corrosion rate, B is the time exponent coefficient, and $d(t)$ is the cross-section thickness loss (in μm). This model adjusts for the variability in the first-year corrosion rate as it cannot be extrapolated in the long term. ISO 9224: 2012 [13] suggests that power law is applicable for up to 20 years, assuming that the growing rust thickness alleviates the corrosion damage. A steady state corrosion with a linear corrosion rate is assumed beyond the 20-year ageing time. Finally, $B = 0.523$ for carbon steel is suggested [13]. Fig. 2 (a) shows the variation of $d(t)$ over time.

Table 1. Corrosion parameters as per ISO 9223: 2012 [11] and pushover analysis results.

Corrosivity Category	**i_{corr} range** (μm/yr)	**Avg.i_{corr}** (μm/yr)	**Mass Loss** η (%)	***Base Shear* for $12\gamma_y$** (kN)	***Base shear Variation* (%)**	**IDR for $12\gamma_y$ (%)**
Pristine	-	-	-	1304		3.03
C3	25-50	37.5	3.7	1191.6	*8.6*	2.9
C4	50-80	65	6.5	1110	*14.90*	2.8
C5	80-200	140	14	895.4	*31.3*	2.53
CX	200-700	300	25	606.3	*53.5*	2.14

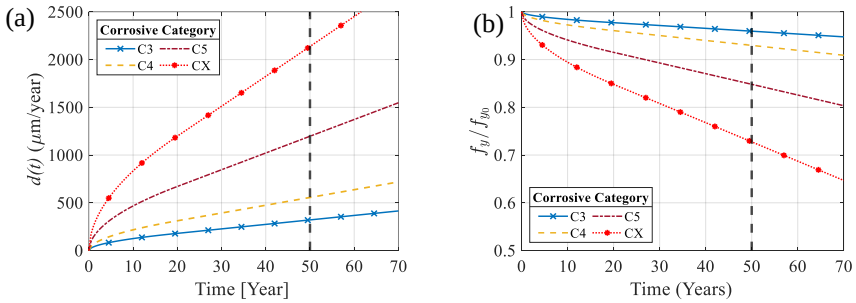

Fig. 2. (a) Thickness loss, $d(t)$ [Eq. (1)], (b) Yield strength degradation [Eq. (2)].

In addition to thickness loss, corrosion deterioration causes degradation of the steel's mechanical properties and is evaluated according to Wang *et al.* (2018) [16]. The degraded parameters [Fig. 2 (b)] are estimated by the percentage mass loss (η), as follows:

$$f_y(t) = f_{yo}[1 - 1.09\eta(t)] \quad (2)$$

where, f_{yo} is the initial yield strength of the steel material. Table 1 provides the mass loss (η) calculated based on thickness loss, $d(t)$, and average i_{corr} for different corrosivity categories. It is to be noted that for CX category, Avg.i_{corr} = 300 μm/year is considered to restrict mass loss up to 25% to consider for the realistic scenarios.

2.3 Finite Element (FE) Modelling

A 2D non-linear FE model of the case-study structure is developed in OpenSees [14]. Columns are modelled using a distributed plasticity approach, while beams are modelled according to a lumped plasticity approach. In addition, panel zones are modelled as per the 'Scissors model' [4]. Beam-to-column connections are assumed to be welded and, therefore, are considered rigid in the FE model. The yield strength (f_y) and elastic modulus (E) are respectively equal to f_y= 344.74 MPa and E = 199.95 GPa. A damping ratio of ζ = 3% is adopted by using mass and stiffness proportional damping (*i.e.*, Rayleigh Damping). Additionally, a leaning column is modelled to account for the P-Δ effects generated by the loads applied on the gravity frame. Additional information is found in Gutiérrez-Urzúa *et al*. (2021) [2] and Gutiérrez-Urzúa and Freddi (2022) [17].

For the 50-year frame, the column sections in the FE model are revised to account for the thickness loss calculated as per Eq. (1) for each corrosivity category. The rotational spring properties modelled as per the 'Scissors model' are revised based on $d(t)$ for column sections. Degradation in the mechanical properties of steel is accounted for following Eq. (2). Column sections are assumed to undergo uniform corrosion along the full length. In this investigation, beam deterioration is not accounted for due to partial protection provided by the slab and its interior location within the building. Additionally, given their non-seismic design and weak panel zones, any deterioration in beams has minimal influence on the lateral strength of the frame under consideration.

3 Seismic performance assessment

3.1 Pushover analysis

Non-linear pushover analysis with the distribution of lateral loads defined according to the first mode is performed to evaluate the lateral strength over a 50-year period under different corrosion levels. Fig. 3 illustrates the response of both pristine and corroded frames in terms of base shear versus first-storey interstorey drift ratio (*IDR*). The percentage variations in lateral strength indicated by base shear corresponding to collapse limit state of the panel zone across different corrosivity categories for the 50-year corroded frames are illustrated in Table 1. The collapse limit for panel zone deformation is considered as 12 times its yield rotation,=$12\gamma_y$ (refer section 3.2). Notably, a mass loss of 3.72% results in an 8.61% reduction in lateral shear strength, while extreme CX conditions lead to over 53.5% strength loss with a ~25% mass loss. A significant reduction in the deformation capacity of the frame is observed in terms of *IDR* for the

collapse limit state of panel zones. In addition, a minor stiffness loss is observed (Fig. 3), leading to a slight fundamental period elongation, *i.e.*, $T_{1,pristine}$ =1.88 sec and $T_{1,CX}$ =2.07 sec (pristine *vs.* 50-year frame -CX exposure).

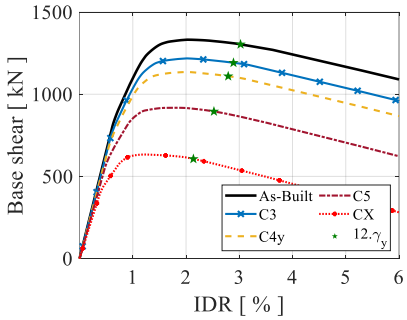

Fig. 3. Base shear *vs. IDR* for the 1st storey for different corrosivity categories.

3.2 Engineering Demand Parameters (*EDP*) and Intensity Measure (*IM*)

Local and global *EDPs* are adopted to evaluate the seismic performance. The local *EDPs* under consideration include the beams' chord rotation (θ_b), column chord rotation (θ_c), and panel zone shear strain (γ). On the other hand, the maximum interstorey drift ratio (*MIDR*), which provides a synthetic description of the seismic response, is used as global *EDP*. Capacity limits for the considered local *EDPs* are conventionally defined based on yield capacity parameters, as previously done by the authors [4].

For the chosen *EDPs*, the ASCE 41-17 [18] provides three different limit states (LSs), namely: (1) Immediate Occupancy (*LS1*), (2) Life Safety (*LS2*), and (3) Collapse Prevention (*LS3*). The details of these capacity limits are summarised in Table 2. Additionally, the capacity limits for the *MIDR* are assumed equal to 0.7% (*LS1*), 2.5% (*LS2*), and 5% (*LS3*) according to the ASCE 41-07 [19]. The interested reader can refer to Gutiérrez-Urzúa *et al.* (2021) [2] and Lad *et al.* (2023) [4] for additional details.

Table 2. Component-level plastic rotation capacity limit states (*LS*) as per ASCE 41-17 [18].

Element	Dimensionless axial load limits	Slenderness limits	Plastic rotation capacity limits		
			LS1	***LS2***	***LS3***
Columns*	$\lvert\nu_G\rvert \leq 0.6$	All	$0.5\,a$	$0.75b$	b
Panel Zone	$\lvert\nu_G\rvert < 0.4$	-	$1\,\gamma_y$	$12\,\gamma_y$	$12\,\gamma_y$

Notes: * 'a' and 'b' are defined in Table 9-7.1 of the ASCE 41-17 [18].

The stiffness reduction generates a slight period elongation of the corroded frame. Thus, to allow the comparison of the seismic response at different stages, the average spectral acceleration ($S_{a,avg}$) between the fundamental time periods of the stiffest and most flexible frames, *i.e.*, $T_{1,pristine}$ and $T_{1,CX}$ is used as *IM* in this study. $S_{a,avg}$ is defined as the geometric mean of accelerations between $T_{1,pristine}$ and $T_{1,CX}$, given by:

$$S_{a,avg}\left(T_{1,pristine} - T_{1,CX}, \zeta = 3\%\right) = \left[\prod_{i=1}^{n} S_a\left(T_{1,n}\right)\right]^{\frac{1}{n}} \quad (3)$$

where n is the number of discrete spectral ordinates between $T_{1,pristine}$ and $T_{1,CX}$. The adopted $S_{a,avg}$ allows for the direct comparison of the fragility curves for the pristine and corroded frames under varied corrosivity categories.

3.3 Non-linear Time History Analyses (NLTHA)

The NLTHA results of the pristine and corroded frames under a single GM record with *IM* = 0.4g are presented in this section. Fig. 4 (a) illustrates the first-storey drift response comparing the pristine and corroded frames. Similarly, Fig. 4 (b) displays the normalised rotation with respect to its yielding value (γ/γ_y) for panel zone *PZ9* (Fig. 1).

It can be highlighted from Table 3 that a small increase in the mass loss (η) causes a significant increase in *MIDR*. Also, from Fig. 4 (a), it can be inferred that the residual *IDR* increases substantially at the end of the selected GM, representing large sustained plastic deformation. This phenomenon can be attributed to the large plastic deformation in the panel zone. Fig. 4 (b) shows residual panel zone deformations (γ/γ_y) ranging from 5 to 28 times for C3 to CX corrosivity category. It is worth mentioning that the results in Fig. 4 are representative of a scenario with sustained residual deformations.

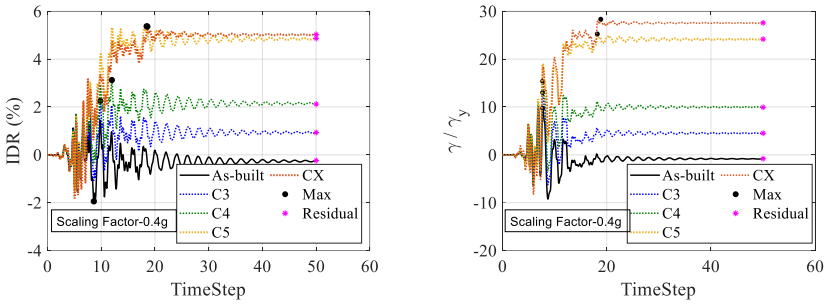

Fig. 4. Time history response: (a) first-storey *IDR* (%), (b) panel zone rotation *PZ9* (γ/γ_y).

Table 3. Non-linear time history (NLTHA) results for the first-storey peak *IDR* and panel zone rotation (*PZ9*) for the pristine and corroded frames (see also Fig. 4).

EDPs	**Pristine**	**C3**	**C4**	**C5**	**CX**
Max $\boldsymbol{\gamma/\gamma_y}$	9.76	13	15.4	25.3	28.3
% variation	-	*33.2%*	*57.8%*	*159.3%*	*190.0%*
MIDR	1.94	2.25	3.13	5.37	5.36
% variation	-	*16.0%*	*61.4%*	*176.9%*	*176.3%*

3.4 Incremental Dynamic Analyses (IDAs) and fragility curves

A suite of 43 far-field GM records was used to perform IDAs. These GMs are not site-specific; thus, this study intends to assess the seismic performance representing a generalised seismic hazard. The selected GMs are scaled to *IM* ranging from 0.1g to 1g.

Fragility curves are derived by comparing the generated *EDPs-IM* pairs for the local- and global-level *EDPs*. Fragility curves describe the probability of exceeding a specified *LS*, conditional to the strong-motion shaking severity, quantified by an appropriately selected *IM*. For each type of *EDP* under consideration (*i.e.*, column' chord rotation - θ_c, panel zone shear strain – γ, and *MIDRs*), and for each GM, the maximum response monitored among all components is considered as a demand sample. On the other hand, code-based capacity limits (ASCE 41-17 [18]) are used to compare with the demand values and, hence, to define fragility curves.

While accounting for the uncertainty in seismic demand (*i.e.*, record-to-record variability), the variation of demand- and deterioration-dependent capacity values is implicitly considered in this study (*i.e.*, θ_y in beams, columns, and panel zones). Other sources of uncertainty are neglected. The deterioration-dependent capacity variation is based on the degradation of the geometrical and mechanical properties over time [4].

Successively, numerical fragility curves are approximated by analytical lognormal curves obtained through least-square minimisation. For the sake of brevity, the results of the beam rotation (θ_b) and *MIDR* are not presented. Fig. 5 provide the fragility curve for the pristine and 50-year corroded frame under different corrosivity categories for column rotation (θ_c) and panel zone rotation (γ), respectively. Table 4 reports the median (med) and dispersion (β) of the lognormal fragility curves for the pristine and 50-year corroded frames considering exposure C3 to CX and their percentile variations.

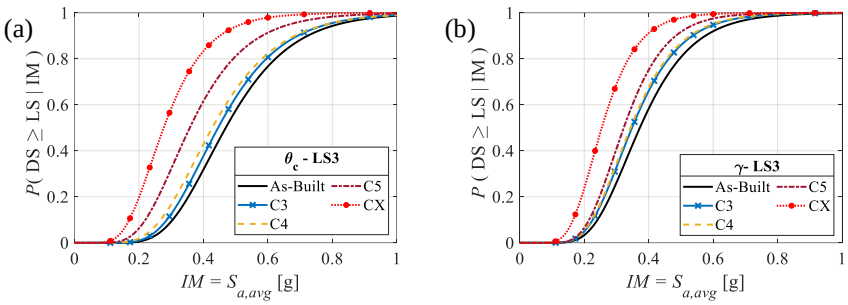

Fig. 5. Fragility curves for (a) column rotation (θ_c), and (b) panel zone rotation (γ).

Table 4. Lognormal fragility curves parameters for pristine and 50-year corroded frames.

LS3	**Pristine**	**C3**	**C4**	**C5**	**CX**
Mass loss (η)	-	3.7%	6.5%	14%	25%
Column (med)	4.61	4.38	4.11	3.51	2.72
med % variation	-	*5.0%*	*10.9%*	*23.8%*	*41.0%*
Dispersion (β)	0.33	0.34	0.36	0.38	0.38
Panel Zone (med)	3.66	3.42	3.38	3.17	2.5
med % variation	-	*6.6%*	*7.7%*	*13.4%*	*31.7%*
Dispersion (β)	0.33	0.33	0.34	0.32	0.34

It can be seen from Fig. 5 and Table 4 that the fragility of column rotation (θ_c) and panel zone rotation (γ) for *LS3* increases significantly with increasing corrosivity compared to the pristine frame. For instance, in the case of column rotation, the median

value decreases by 23.8% and 41% for a mass loss (η) of 14% and 25%. Additionally, the dispersion (β) values show small increasing trend for column rotation while no change is observed for panel zone rotation. The results for other limit states for column and panel zone rotation show similar trends but not presented due to space limitations. At the global level, *MIDR* shows a similar increase in failure probability. For the beam rotation, fragility increases for *LS1*, while there is negligible variation for *LS2* and *LS3*.

Comparing the fragilities of columns and panel zone rotations in Fig. 5, it can be observed that columns show higher variations for all corrosivity categories. Consequently, higher corrosion intensity leads to a non-linear increase in seismic fragility for low-code steel MRF. Thus, steel MRFs built in highly corrosive environments can experience significant damage or premature collapse under seismic events compared to low corrosive environments, leading to a reduction in the service life of the steel MRFs.

4 Conclusion

Low-code steel structures are often characterised by low ductility and, hence, limited seismic performance. Moreover, they are susceptible to atmospheric corrosion degradation under corrosive environments, further increasing their seismic vulnerability. The current study examines the seismic performance of a non-seismically designed (low-code) existing steel moment resisting frame (MRF) under the influence of atmospheric corrosion deterioration for a 50-year ageing time, considering different corrosivity categories. An OpenSees finite element (FE) model was developed to perform non-linear quasi-static and dynamic analyses for fragility derivation. This study accounts for global and local engineering demand parameters (*EDPs*) to evaluate the seismic performance of the frame after corrosion deterioration.

Different corrosivity categories representing the varied intensity of corrosive environments are adopted as per ISO 9223:2012. Atmospheric corrosion's primary and secondary effects were quantified based on the recommendations of ISO 9224:2012 and incorporated in the FE model as uniform corrosion on steel members. The results of the quasi-static analysis revealed that a mass loss of 3.7%, 6.5%, 14%, and 25% causes a reduction of 8.6%, 14.9%, 31.3% and 53.5%, respectively, in the lateral strength of the frame. Conversely, only a minor reduction in the stiffness of the case-study frame was observed. Incremental Dynamic Analyses (IDAs) were successively performed using a suite of 43 ground motion records to assess the seismic performance accounting for the influence of the earthquake input's uncertainty. Fragility curves are derived for global- and local-level *EDPs* considering code-based capacity limits for three limit states (*LSs*). The fragility assessment highlights that panel zones and columns show a significant increase in the failure probability under increasing corrosivity categories. This may lead to substantial damage, change in failure modalities, or collapse under an earthquake event. With heightened corrosion intensities, the service life of the steel MRFs is significantly diminished. The results provide a good comparison of the evolution of seismic fragility under varied corrosive environments. Future works will examine more realistic corrosion degradation- pitting corrosion and its distribution, stress-induced corrosion beam-column joints, and uncertainty in corrosion estimations.

References

[1] Gupta A. Seismic demands for performance evaluation of steel moment resisting frame structures. Stanford University; 1999.

[2] Gutiérrez-Urzúa F, Freddi F, Di Sarno L. Comparative analysis of code-based approaches for seismic assessment of existing steel moment resisting frames. Journal of Constructional Steel Research 2021;181:106589.

[3] Wang H, Wang Y, Zhang Z, Liu X, Xu S. Cyclic behavior and hysteresis model of beam-column joint under salt spray corrosion environment. Journal of Constructional Steel Research 2021;183:106737.

[4] Lad D, Freddi F, Ghosh J, Rossetto T. Impact of corrosion deterioration on the seismic performance of steel frame structures, Society for Earthquake and Civil Engineering Dynamics (SECED); 2023.

[5] Mortagi M, Ghosh J. Concurrent modelling of carbonation and chloride-induced deterioration and uncertainty treatment in aging bridge fragility assessment. Structure and Infrastructure Engineering 2020;18:197–218.

[6] Shekhar S, Ghosh J, Ghosh S. Impact of Design Code Evolution on Failure Mechanism and Seismic Fragility of Highway Bridge Piers. J Bridge Eng 2020;25:04019140.

[7] Shekhar S, Freddi F, Ghosh J, Lad D. Influence of corrosion on failure modes and lifetime seismic vulnerability assessment of low-ductility RC frames. Earthquake Engineering & Structural Dynamics 2023;52:5162–84.

[8] Dizaj EA, Madandoust R, Kashani MM. Probabilistic seismic vulnerability analysis of corroded reinforced concrete frames including spatial variability of pitting corrosion. Soil Dynamics and Earthquake Engineering 2018;114:97–112.

[9] Zhang X, Zheng S, Zhao X, Yang Q. Seismic performance and hysteretic model of corroded steel frame columns in offshore atmospheric environment. Advances in Structural Engineering 2023;26:3041–64.

[10] Di Sarno L, Majidian A, Karagiannakis G. The Effect of Atmospheric Corrosion on Steel Structures: A State-of-the-Art and Case-Study. Buildings 2021;11:571.

[11] ISO 9223: 2012. Corrosion of metals and alloys—corrosivity of atmospheres—classification, determination and estimation. The British Standard Institute 2012.

[12] Zhang X, Zheng S, Zhao X. Experimental and numerical study on seismic performance of corroded steel frames in chloride environment. Journal of Constructional Steel Research 2020;171:106164.

[13] ISO 9224: 2012(E). Corrosion of Metals and Alloys – Corrosivity of Atmospheres – Guiding Values for the Corrosivity Categories. International Standards Organization, Geneve 2012.

[14] McKenna F, Fenves GL, Scott MH, others. Open system for earthquake engineering simulation. University of California, Berkeley, CA 2000.

[15] Minimum Design Loads for Buildings and Other Structures, ASCE/SEI 7-10. American Society of Civil Engineers; 2013.

[16] Wang H, Xu S, Li A, Kang K. Experimental and numerical investigation on seismic performance of corroded welded steel connections. Engineering Structures 2018;174:10–25.

[17] Gutiérrez-Urzúa F, Freddi F. Influence of the design objectives on the seismic performance of steel moment resisting frames retrofitted with buckling restrained braces. Earthq Engng Struct Dyn 2022;51:3131–53.

[18] Seismic Evaluation and Retrofit of Existing Buildings, ASCE/SEI 41-17. American Society of Civil Engineers; 2017.

[19] Seismic Rehabilitation of Existing Buildings, ASCE/SEI 41-06. American Society of Civil Engineers; 2007.